EEG-Based Motor Imagery Classification Using Multilayer Perceptron Neural Network

S.K.S. Ferreira[1], A.S. Silveira[2] and A. Pereira[1]

[1] Institute of Technology, Federal University of Pará, Belém, Brazil
[2] Laboratory of Control and Systems, Federal University of Pará, Belém, Brazil

Abstract— **Signals derived from brain activity can be used as commands to control an external device or application in Brain-Computer Interface (BCI) systems. Electroencephalography (EEG) is widely used to record brain signals due to its non-invasive nature, relatively low-cost, and high temporal resolution. BCI performance depends on choices regarding available options for signal pre-processing, classifiers, and feature extraction techniques. In this paper, we describe the use of an Artificial Neural Network (ANN) based on a Multilayer Perceptron (MLP) architecture as a classifier to identify motor imagery tasks using EEG signals from nine subjects of an experimental data set. BCIs based on brain signals recorded during motor imagery tasks use the changes in amplitude of specific cortical bands as features. Moreover, we evaluated the effect of systematically decreasing the number of inputs (EEG channels) on the classifier performance. The results show that a MLP classifier was able to segregate the EEG signature of four motor imagery tasks with at least 70% accuracy using at least 12 EEG channels.**

Keywords— **Motor Imagery, MLP, Periodogram, DWT.**

I. Introduction

Motor Imagery is a mental task in which subjects imagines themselves performing motor actions without actually moving their body. This type of imagery activates the same cortical motor areas as during the performance of real movement (cortical activation) [1]. Electroencephalography (EEG) signals recorded during motor imagery tasks can be used to implement brain-computer interfaces, as well as for motor rehabilitation protocols [2].

During motor imagery, Event-Related Desynchronization (ERD) and Event-Related Synchronization (ERS) can be observed in the mu ($8-12$ Hz) and beta rhythms ($13-30$ Hz) of the EEG signal [3]. The mu rhythm is related to alpha activity over the sensorimotor cortex. Desynchronization indicates suppression of oscillatory activity (energy decreases) in a particular frequency band whereas the synchronization refers to an increase of oscillatory activity. These changes in the amplitude of specific EEG bands have been used as input for Brain-Computer Interface (BCI) systems [4, 5]. In additional to mu and beta, previous works have also included the delta rhythm ($0.5-4$ Hz) [6].

The elicited ERD/ERS patterns are topographically organized along the cortical surface. Hence, BCI-related motor imagery usually includes limb and tongue movements, due to the fact that these movements engage relatively large cortical areas and are easier to be isolated with surface EEG electrodes [7]. In particular, the pattern of brain activation during motor imagery of hand movements is lateralized: motor imagery of the left (right) hand causes ERD (ERS) in the right (left) sensorimotor cortex, and vice-versa. Thus, the motor imagery of hand movements can be associated with corresponding increase/decrease of EEG energy in the C4/C3 electrodes, which are usually localized over the regions representing hand movements in the sensorimotor cortex [3].

This study investigates the performance of a Multilayer Perceptron (MLP) Artificial Neural Network (ANN) built with 15 neurons in its hidden layer during the classification of four motor imagery tasks: movements of the left hand, the right hand, the feet, and the tongue. In order to test the classifier, we used data of nine subjects obtained from data set A of the BCI Competition IV. The feature We extracted from the dataset was the individual subject's average power of the mu/alpha and beta EEg frequency ranges using periodogram as the spectral estimation method and the Wavelet Energy Spectrum (WES).

We performed three simulations using features extracted from mu, beta, and a combination of both frequency ranges. Also, in order to investigate strategies to reduce computational cost and system complexity, we systematically reduced the number of channel inputs while measuring the effect on performance accuracy [6].

II. Materials and Methods

A. Features extraction

In EEG analysis, power spectral density (PSD) is usually calculated separately for each standard range (e.g. delta, theta, alpha, mu, beta, and gamma) (V^2/Hz) [8].

The periodogram estimates the PSD using the squared-magnitude of the Discrete-Time Fourier Transform (DTFT)

and is defined as:

$$P_x(\omega) = \frac{1}{N}\left|DTFT(x[n])\right|^2 = \frac{1}{N}\left|\sum_{n=0}^{N-1} x[n]e^{-j\omega n}\right|^2 \quad (1)$$

where $P_x(\omega)$ is the PSD, N represents the total number of samples of the EEG signal $x[n]$ from one channel, and ω is the frequency $-\pi < \omega < \pi$. The Fast Fourier Transform algorithm is used to compute DTFT and, as a result, the periodogram [9]. The use of an appropriate window function can reduce smearing and leakage effects.Considering a window function W of length L, the $x_W[n] = W[n]x[n]$ represents a windowed data segment from the EEG signal $x[n]$. Thus, the periodogram (1) of this segment is:

$$P_{xw} = \frac{1}{L}\left|DTFT(x_W[n])\right|^2 = \frac{1}{L}\left|\sum_{n=0}^{L-1} W[n]x[n]e^{-j\omega n}\right|^2 \quad (2)$$

Previous studies indicate that for the spectral analysis of biomedical signals, the most appropriate windows are the rectangular and Hanning [10]. In thw present work, we used a Hanning window of length 250 to compute the periodogram of each data segment, with a bin size of 100 *ms* (25 samples).

By integrating the PSD within a frequency range, we can obtain the average power contained in this frequency interval. In the present work, the area under the curve of the PSD of mu/alpha/beta rhythms is decomposed into rectangles to calculate the approximate integral, i.e., the average power of each band.

In addition to average power, we calculated the WES with a Discrete Wavelet Transform (DWT) implementation, which decomposes a signal into multi-levels $j = 1,2,...J$ with respective frequency components and is used especially in EEG signals due to its non-stationary and non-linear characteristics [11]. The DWT is defined as:

$$DWT(j,k) = \frac{1}{\sqrt{|2^j|}}\int_{-\infty}^{\infty} x(t)\,\psi\left(\frac{t-2^j k}{2^j}\right)dt \quad (3)$$

where $x(t)$ is the signal captured at each EEG channel, ψ is a wavelet function, and j is the decomposition level. In this study is used the 4^{th} order Daubechies wavelet (db4).

The DWT implementation developed by [12] involves the use of Low-Pass (LP) and High-Pass (HP) filter pairs called quadrature mirror filters. In the first step, the EEG signal is subject to both LP and HP filters, with cut-off frequency equal to one fourth of the sampling frequency F_s. This step results in the approximation (cA_j) and detail (cD_j) coefficients of the first level ($j = 1$). The same procedure can be repeated until the desired decomposition level is reached.

The EEG signals used in the present work were sampled with 250 Hz (F_s). Following the Nyquist Sampling Theorem $F_s \geq 2F_{max}$, the maximum useful frequency is equal to half of the sampling frequency, i.e., 125 Hz. Thus, as a result of the DWT decomposition, we uncover a relationship between the cD_4 ($7.8125 - 15.625$ Hz) wavelet components and the mu/alpha rhythm and between the cD_3 ($15.625 - 31.25$ Hz) coefficients and the beta rhythm

The WES at scale j and instant k (E_{jk}) is the square of the wavelet transform coefficients $E_{jk} = d_{jk}^2$, where d_{jk} denotes the approximation coefficient cA_{jk} or detail coefficient cD_{jk}. The sum of each E_{jk} composes the wavelet spectrum at scale j to cA_{jk} and cD_{jk}. The WES for detail coefficients is described below [13, 14]:

$$E_{detail\,j} = \sum_{k=1}^{\frac{N}{2^j}} \left|cD_{jk}\right|^2 \quad (4)$$

In the present work, the WES of the cD_3 and cD_4 coefficients are obtained with the sliding of the fixed time window [13]. This procedure allows following the variations in wavelet energy over time [15]. Hence, given the wavelet coefficients:

$$D = \left\{d_{jk}, k = 1,2,...,N; j = 1,2,...,J\right\} \quad (5)$$

the sliding-window should be written as:

$$W(m;w,\delta) = \left\{d_{jk}, k = 1+m\delta,...,w+m\delta\right\} \quad (6)$$

where $2 \leq w \leq N$ is the width of window, $1 \leq \delta \leq N$ is the sliding factor, and $m = 0,1,2,...,M$; $M = (N-w)/\delta$ is the number of sliding steps [16, 17]. We used the moving window parameters $w = 33$ and $\delta = 1$ to calculate the wavelet energy of the cD_3 and cD_4 coefficients.

B. Experimental design

We used the data set from the fourth edition of the BCI Competition provided by the University of Graz. This data set consists of EEG signals from 9 healthy subjects performing motor imagery tasks. The signals were sampled with 250 Hz and the electrodes were placed according to the International 10-20 System. Each subject, designated here as Sub_1, Sub_2,..., Sub_9, performed four different imagery tasks: movement of the left hand (Class 1), right hand (Class 2), feet (Class 3), and tongue (Class 4). Two sessions were performed on different days. Each session has 6 runs composed by 48 trials (12 trials per class) and each run is separated by short breaks. The experimental paradigm is represented in Figure 1 [18].

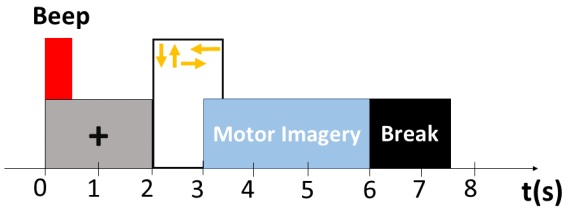

Fig. 1: Experimental Paradigm

As observed in Figure 1, at $t = 0s$, i.e., at the beginning of the trial, a fixation cross is exhibited on a computer screen together with a short acoustic warning (beep). After two seconds ($t = 2s$) a cue in the form of an arrow appears, indicating the motor imagery task: pointing to the left (class 1), right (class 2), down (class 3) or up (class 4). The cue remained on the screen for $1.25s$. The subject should carry out the task until $t = 6s$, when the fixation cross disappeared. At the end of each trial there is a short break.

C. Topology, training, and evaluation of MLP

The MLP used in this study has two layers, i.e., a hidden layer and an output layer and the number of neurons in each layer is 15 and 4, respectively. The number of hidden neurons (15) was chosen in an optimization process aiming at minimizing both the time required for training and the complexity of the classifier, while increasing the accuracy obtained using all channels. In the output layer, class 1 is represented as $[1\,0\,0\,0]^T$, class 2 as $[0\,1\,0\,0]^T$, class 3 as $[0\,0\,1\,0]^T$, and class 4 as $[0\,0\,0\,1]^T$. The training algorithm was the Levenberg-Marquadt Backpropagation [19].

The classification accuracy was evaluated in three scenarios: simulation with features extracted from the mu/alpha rhythm, the beta rhythm, and from both rhythms. A total of five experiments were performed in each scenario with 70% of the data randomly reserved for training and 30% to validation. In addition, the number of EEG channels (n) used as input was systematically reduced in order to analyze the accuracy with low input complexity. The channels selected are detailed below:

- 22 Channels: Fz, FC3, FC1, FCz, FC2, FC4, C5, C3, C1, Cz, C2, C4, C6, CP3, CP1, CPz, CP2, CP4, P1, Pz, P2, and POz.
- 18 Channels: Fz, FC3, FC1, FCz, FC2, FC4, C5, C3, C1, Cz, C2, C4, C6, CP3, CP1, CPz, CP2, and CP4.
- 16 Channels: Fz, FC3, FC4, C3, C1, Cz, C2, C4, CP3, CP1, CP2, CP4, P1, Pz, P2, and POz.
- 14 Channels: Fz, FC1, FCz, FC2, C5, C3, C1, Cz, C2, C4, C6, CP1, CPz, and CP2.
- 12 Channels: FC3, FC4, C5, C3, Cz, C4, C6, CP3, CPz, CP4, P1, and P2.
- 10 Channels: Fz, FCz, C5, C3, C1, Cz, C2, C4, C6, and CPz.
- 8 Channels: Fz, C3, C1, Cz, C2, C4, CPz, and Pz.

The features extracted from those channels, as described in section II, are the WES and the average power in the mu/alpha and beta bands, which were included in the feature vector for each EEG channel. Hence, each subject is associated with four feature matrices for each class, with the same number of samples: the average power matrix in the mu band (1562×22), the average power matrix in the beta band (1562×22), the WES matrix corresponding to the mu band (1562×22), and the WES matrix corresponding to the beta band (1562×22).

Since during the training stage the system is biased to the influence of features with larger values, the features are normalized along the range $[0, 1]$ with *softmax* activation function in both layers of the neural network. In order to evaluate classification performance, the accuracy is calculated based on information from the confusion matrix, given by:

$$A_c = \left(\frac{T_N + T_P}{T_N + T_P + F_N + F_P} \right) \times 100 \tag{7}$$

where T_N is the number of true negatives, T_P of the true positives, F_N of the false negatives, and F_P of the false positives. An accuracy higher than 70% is suggested for BCI applications [20].

III. Results and Discussion

In the present work, we used an MLP neural network to classify four types of motor imagery performed by 9 subjects based on spectral estimation and WES. Figure 2 and 3 shown the features extracted before and during motor imagery (MI), considering C3 channel for average band power and C4 channel for WES, of the subject 5.

Analyzing the results of each simulation, it is possible to see that the ANN reaches significant performance using only the mu/alpha frequency (up to 94.06 ± 1.37 using all electrodes), as can see in Table 1. Also, the minimum number of channels needed to obtain at least 70% accuracy was at least 12 channels for simulations considering separately mu and beta rhythms (Tables 1 and 2), and at least 14 channels for simulation using the features vector in both rhythms (Table

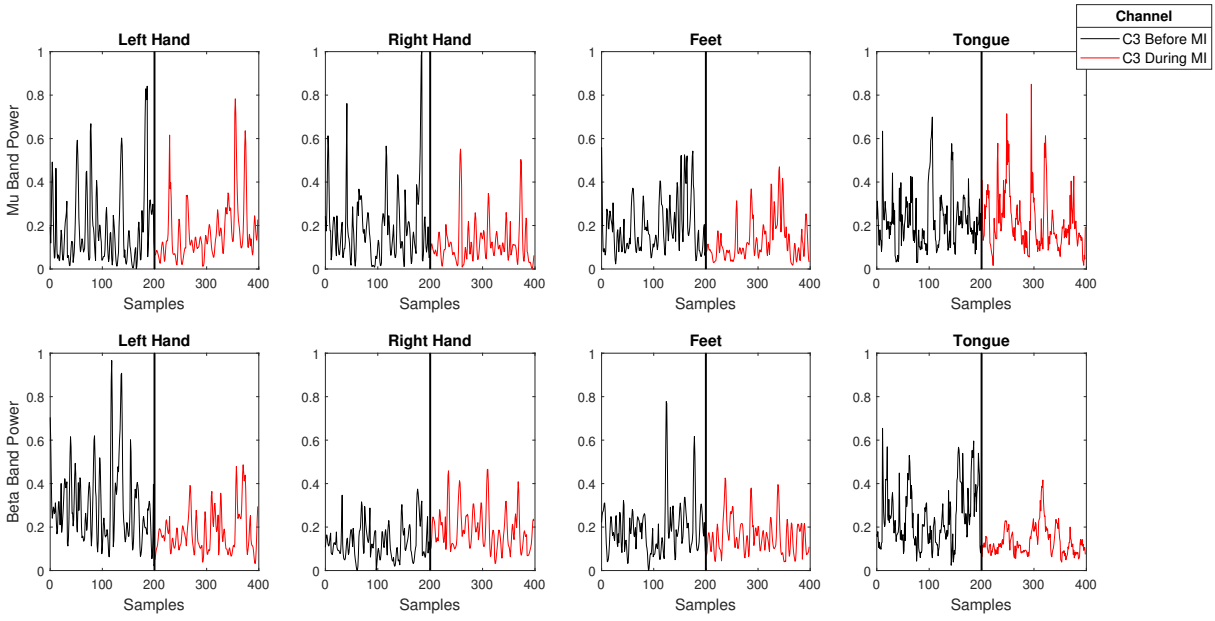

Fig. 2: Normalized average power in the mu/alpha and beta bands of the Subject 5

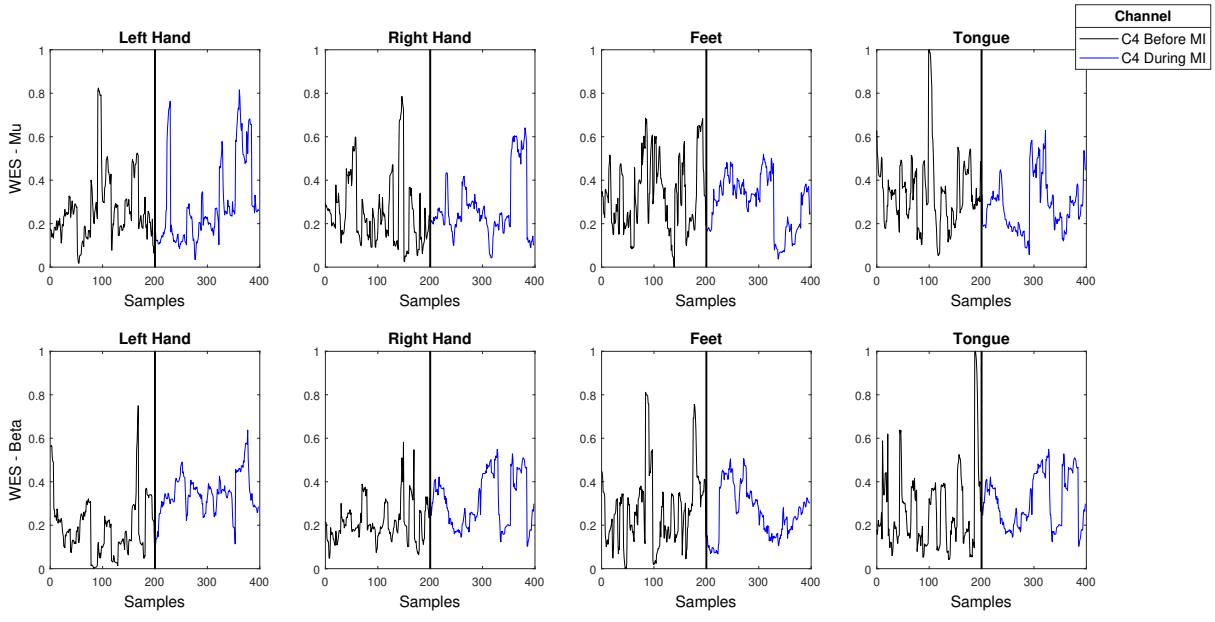

Fig. 3: Normalized WES in the mu/alpha (cD_4) and beta (cD_3) bands of the Subject 5

3). Therefore, the level of classification accuracy using alpha or beta reaches higher values than the use of the two rhythms together and enables a reduction of at least 10 EEG channels.

Furthermore, comparing the simulations results using mu/alpha rhythm and the simulations using beta rhythm, for $n = 22$, we found a greater classification accuracy for features extracted in the alpha band than for beta band, for most subjects, indicating differences in the degree of desynchronization of sensorimotor rhythms.

Other similar studies with ANN includes the use of aver-

age power and wavelet energy spectrum, such as [21], which report accuracy equal to 77.1429% using average power and 83.5714% using WES, for two classes of motor imagery. In additional, [6] achieved 80 ± 10 of accuracy using ANN for classification of two classes of motor imagery, and after filtration and analysis of channel reduction, the accuracy enhances to 90 ± 5 using 8 electrodes.

IV. Conclusion

This paper presented a study about the use of MLP to classify EEG signals based on motor imagery tasks, using features that can identify the energy modulation that occurs during this type of mental activity. The technique involves the average power, derived from the periodogram method, and the windowed wavelet energy spectrum, in order to characterize the ERD/ERS during four motor imagery tasks. It is possible to conclude that, using the BCI data set, the implementation of a MLP for classification tasks with 15 hidden neurons and two layers has enough accuracy using all 22 electrodes. Moreover, the channel reduction analysis performed has shown the possibility to use fewer EEG channels than available, maintaining enough accuracy.

Conflict of Interest

The authors declare that they have no conflict of interest.

Acknowledgements

To Laboratory of Control and Systems (LACOS-UFPA) and Neuroprocessing Laboratory (LABNEP-UFPA).

A.S. Silveira acknowledges the financial support of the *Conselho Nacional de Desenvolvimento Científico e Tecnológico* under grant 408559/2016-0.

References

1. Mulder T. Motor imagery and action observation: cognitive tools for rehabilitation. *J Neural Transm.* 114(10):1265–1278 (2007).
2. Padfield N, Zabalza J, Zhao H et al. EEG-based brain-computer interfaces using motor-imagery: Techniques and challenges. *Sensors.* 19(6):1423 (2019).
3. Pfurtscheller G, Neuper C. Motor imagery activates primary sensorimotor area in humans. *Neurosci. Lett.* 239(2-3):65–68 (1997).
4. Zuo C, Jin J, Yin E et al. Novel hybrid brain-computer interface system based on motor imagery and P300. *Cogn. Neurodyn.* 14(2):253–265 (2020).
5. Abdalsalam E, Yusoff M, Malik A et al. Modulation of sensorimotor rhythms for brain-computer interface using motor imagery with online feedback. *Signal Image Video Process.* 12(3):557–564 (2018).
6. Maksimenko V, Kurkin S, Pitsik E et al. Artificial neural network classification of motor-related eeg: An increase in classification accuracy by reducing signal complexity. *Complexity.* 2018 (2018).
7. Graimann B, Allison B, Pfurtscheller G. Brain–computer interfaces: A gentle introduction. In *Brain-computer interfaces*, pp 1–27. Springer (2009).
8. Zhang Z. Spectral and Time-Frequency Analysis. In *EEG Signal Processing and Feature Extraction*, pp 89–116. Springer (2019).
9. Mello C. *Biomedical Engineering*. BoD–Books on Demand (2009).
10. Akin M, Kiymik M K. Application of periodogram and AR spectral analysis to EEG signals. *J Med Syst.* 24(4):247–256 (2000).
11. Thampi S M, Gelbukh A, Mukhopadhyay J. *Advances in signal processing and intelligent recognition systems*. Springer (2014).
12. Mallat S G. A theory for multiresolution signal decomposition: the wavelet representation. *IEEE Trans. Pattern Anal. Mach. Intell.* 11 (1987).
13. Zheng-You H E, Xiaoqing C, Guoming L. Wavelet entropy measure definition and its application for transmission line fault detection and identification. In *International Conference on Power System Technology* , pp 1–6 IEEE (2006).
14. Kumar Y, Dewal M L, Anand R S. Relative wavelet energy and wavelet entropy based epileptic brain signals classification. *Biomed Eng Lett.* 2(3):147–157 (2012).
15. He A. Fault detection of traction power supply system based on wavelet energy entropy. In *AIP Conference Proceedings* 2066(1) AIP Publishing LLC (2019).
16. Chen J, Li G. Tsallis wavelet entropy and its application in power signal analysis. *Entropy.* 16(6):3009–3025 (2014).
17. Yang Q, Wang J. Multi-level wavelet shannon entropy-based method for single-sensor fault location. *Entropy.* 17(10):7101–7117 (2015).
18. Brunner C, Leeb R, Müller-Putz G, Schlögl A et al. BCI Competition 2008–Graz data set A. *Institute for Knowledge Discovery (Laboratory of Brain-Computer Interfaces), Graz University of Technology.* (2008).
19. Rashid M M, Ahmad M. Classification of motor imagery hands movement using levenberg-marquardt algorithm based on statistical features of EEG signal. In *3rd International Conference on Electrical Engineering and Information Communication Technology (ICEEICT)* , pp 1–6 (2016).
20. Kübler A, Kotchoubey B, Kaiser J et al. Brain–computer communication: Unlocking the locked in. *Psychol. bull.* 127(3):358 (2001).
21. Chatterjee R, Bandyopadhyay T. EEG based Motor Imagery Classification using SVM and MLP. In *2nd International Conference on Computational Intelligence and Networks (CINE)* , pp 84–89 (2016).

Table 1: Average accuracy for MLP using features extracted within *mu* frequency range.

Subject	$n = 22$	$n = 18$	$n = 16$	$n = 14$	$n = 12$	$n = 10$	$n = 8$
Sub_1	**91.96 ± 0.28**	78.24 ± 1.85	78.78 ± 3.64	76.25 ± 0.96	77.07 ± 3.13	69.57 ± 0.86	59.99 ± 1.44
Sub_2	**93.16 ± 1.09**	**81.90 ± 1.96**	**82.35 ± 1.61**	**80.79 ± 0.88**	75.72 ± 0.93	69.33 ± 1.00	63.34 ± 1.54
Sub_3	**95.19 ± 0.34**	**80.36 ± 1.60**	**88.25 ± 4.56**	**82.65 ± 1.67**	71.79 ± 1.38	69.64 ± 0.93	69.54 ± 1.78
Sub_4	**94.62 ± 0.23**	**86.03 ± 1.01**	78.52 ± 1.45	**82.19 ± 1.60**	76.33 ± 0.95	70.49 ± 1.29	72.02 ± 0.61
Sub_5	**94.95 ± 0.51**	**85.62 ± 1.29**	**79.08 ± 1.53**	**81.43 ± 1.62**	75.50 ± 1.75	70.11 ± 1.42	72.08 ± 1.36
Sub_6	**95.04 ± 1.08**	**90.49 ± 0.87**	**81.64 ± 1.25**	**82.40 ± 2.37**	76.21 ± 1.58	74.69 ± 0.25	65.50 ± 2.16
Sub_7	**95.05 ± 0.40**	**79.44 ± 1.06**	**87.50 ± 0.82**	**80.81 ± 1.86**	73.96 ± 1.57	72.86 ± 3.28	70.12 ± 0.83
Sub_8	**94.79 ± 0.58**	**82.47 ± 2.71**	**83.17 ± 1.21**	**84.33 ± 0.45**	78.20 ± 1.23	**79.40 ± 2.68**	70.15 ± 1.96
Sub_9	**91.82 ± 1.03**	**82.24 ± 2.67**	**81.52 ± 3.17**	73.89 ± 2.03	58.27 ± 1.40	63.25 ± 1.95	61.70 ± 1.03
$\mu \pm \sigma$	**94.06 ± 1.37**	**82.98 ± 3.82**	**82.31 ± 3.56**	**80.53 ± 3.33**	**73.67 ± 6.06**	71.04 ± 4.41	67.16 ± 4.61

Table 2: Average accuracy for MLP using features extracted within *beta* frequency range.

Subject	$n = 22$	$n = 18$	$n = 16$	$n = 14$	$n = 12$	$n = 10$	$n = 8$
Sub_1	**95.66 ± 0.29**	**91.34 ± 2.38**	**85.62 ± 0.91**	**88.84 ± 0.99**	78.14 ± 1.16	72.38 ± 2.53	68.98 ± 1.85
Sub_2	**93.00 ± 0.75**	**81.23 ± 0.88**	**80.36 ± 2.46**	73.28 ± 3.13	68.85 ± 0.71	67.78 ± 1.61	63.47 ± 0.60
Sub_3	**87.54 ± 2.54**	78.49 ± 2.82	77.03 ± 1.82	73.68 ± 2.32	69.14 ± 1.55	64.46 ± 2.89	64.52 ± 1.13
Sub_4	**97.00 ± 0.19**	**93.78 ± 0.52**	**86.12 ± 4.41**	**82.94 ± 2.57**	78.57 ± 2.60	73.72 ± 3.63	66.45 ± 1.37
Sub_5	**96.30 ± 0.90**	**82.74 ± 9.36**	**86.66 ± 4.24**	**80.66 ± 1.07**	78.78 ± 1.26	74.64 ± 2.75	66.70 ± 2.52
Sub_6	**92.03 ± 1.61**	77.00 ± 0.47	**85.72 ± 1.90**	75.53 ± 3.16	70.43 ± 0.81	68.22 ± 0.71	63.30 ± 1.18
Sub_7	**92.32 ± 2.06**	**79.53 ± 2.52**	**81.42 ± 2.93**	72.71 ± 1.68	75.18 ± 1.66	66.32 ± 1.95	63.56 ± 3.49
Sub_8	**89.02 ± 0.84**	**79.17 ± 1.37**	74.52 ± 1.46	63.35 ± 2.28	69.77 ± 1.87	59.06 ± 1.33	54.50 ± 0.33
Sub_9	**86.85 ± 1.26**	**80.68 ± 1.39**	78.19 ± 1.30	**79.97 ± 1.06**	72.00 ± 0.96	70.91 ± 1.08	70.20 ± 1.11
$\mu \pm \sigma$	**92.19 ± 3.76**	**82.66 ± 5.88**	**81.74 ± 4.52**	**76.46 ± 6.97**	**73.43 ± 4.24**	68.61 ± 4.96	64.63 ± 4.53

Table 3: Average accuracy for MLP using features extracted within *mu* and *beta* rhythms.

Subject	$n = 22$	$n = 18$	$n = 16$	$n = 14$	$n = 12$	$n = 10$	$n = 8$
Sub_1	**89.59 ± 0.70**	77.95 ± 2.24	71.72 ± 1.39	77.03 ± 0.47	71.61 ± 1.29	63.10 ± 1.01	58.35 ± 0.60
Sub_2	**86.34 ± 0.84**	74.42 ± 1.08	75.07 ± 1.09	65.66 ± 2.75	70.40 ± 2.04	60.61 ± 1.90	55.25 ± 0.57
Sub_3	**87.55 ± 1.09**	70.11 ± 3.57	69.45 ± 2.57	66.98 ± 0.97	62.61 ± 2.93	61.04 ± 1.46	65.10 ± 0.87
Sub_4	**90.57 ± 1.67**	**81.22 ± 2.14**	76.58 ± 3.30	77.41 ± 4.25	77.96 ± 2.37	66.84 ± 2.96	56.76 ± 1.36
Sub_5	**91.78 ± 1.00**	**81.66 ± 1.91**	76.07 ± 1.51	**79.43 ± 2.25**	70.87 ± 1.81	64.70 ± 3.65	57.95 ± 0.75
Sub_6	**91.26 ± 1.22**	76.32 ± 1.87	78.40 ± 0.94	70.86 ± 1.46	67.95 ± 1.11	64.49 ± 0.75	58.29 ± 0.74
Sub_7	**90.91 ± 0.43**	74.50 ± 1.17	**81.01 ± 1.37**	71.74 ± 1.24	71.71 ± 1.38	67.30 ± 1.20	62.15 ± 2.02
Sub_8	**87.72 ± 1.62**	75.44 ± 1.36	72.67 ± 1.06	71.93 ± 0.89	63.36 ± 2.12	61.05 ± 1.79	57.93 ± 1.94
Sub_9	**85.08 ± 0.89**	76.87 ± 1.07	72.16 ± 1.81	66.89 ± 0.97	60.34 ± 1.66	63.89 ± 0.80	55.78 ± 2.26
$\mu \pm \sigma$	**88.98 ± 2.38**	**76.50 ± 3.56**	**74.79 ± 3.64**	**71.99 ± 5.03**	68.53 ± 5.55	63.67 ± 2.46	58.62 ± 3.13

Author: Shirley Karolina da Silva Ferreira
Institute: Institute of Technology (ITEC)
Street: R. Augusto Côrrea
City: Belém
Country: Brazil
Email: shirley.ferreira@itec.ufpa.br